IOP PUBLISHING CLASSICAL AND QUANTUM GRAVITY

Class. Quantum Grav. **24** (2007) 5869–5887 doi:10.1088/0264-9381/24/23/010

Spurious acceleration noise in spaceborne gravitational wave interferometers

Patricia Purdue[1] **and Shane L Larson**[2]

[1] Department of Physics, Colorado College, Colorado Springs, CO 80903, USA
[2] Department of Physics, Weber State University, Ogden, UT 84408, USA

Received 1 July 2007, in final form 6 September 2007
Published 21 November 2007
Online at stacks.iop.org/CQG/24/5869

Abstract

An important source of noise in the Laser Interferometer Space Antenna (LISA) is residual acceleration on the proof masses at the heart of the interferometer system. Two proof masses are carried by each sciencecraft in the LISA constellation, oriented along each of two laser links that are maintained between the distant partners in the constellation. Any change in the local mass distribution will create spurious forces on the individual proof masses which will have to be understood as part of the data analysis reduction. This paper considers the general case of accelerations on the individual proof masses in three dimensions for perturbing masses passing by a LISA sciencecraft with arbitrary velocity vectors and impact parameters. Encounters of this kind are impulsive, occurring over short time scales and appearing in the data record as bursts. The formalism is then applied in a few sample cases, including a meteor fly-by and a thruster maneuver.

PACS numbers: 04.80.Nn, 04.80.−y, 95.55.Ym, 07.87.+v

1. Introduction

Space-based gravitational wave observatories such as the proposed LISA (Laser Interferometer Space Antenna) mission will be subject to a variety of sources of noise which ultimately limit their sensitivity to faint astrophysical gravitational wave signals. At low frequencies, the dominant source of noise will be spurious accelerations on the individual proof masses of an individual LISA sciencecraft. Most general treatments of the LISA sensitivity assume a steady background level of noise which will define a limiting threshold for the detection of signals [1–4]. For the general background of acceleration noise (e.g., noise due to space weather effects such as fluctuating solar irradiance) this treatment should be adequate, but there are plausible cases where short bursts of acceleration will be imparted to the instrumentation on a LISA sciencecraft. Examples include the nearby passage of dust grains, the repositioning of an onboard communications antenna, or a shift in the center of mass of the sciencecraft with

respect to the proof masses as part of the drag-free system. Events like these can produce strong fluctuations and bursts of noise that are capable of fooling data analysis algorithms by producing false detections. Estimates [5] suggest that, for high confidence levels in some gravitational wave detection searches, only limited rates of bursting noise can be tolerated. It is thus important to characterize different sources of burst noise in an effort to build analysis algorithms that mitigate false detections.

Acceleration events also play an important role in the 'data gap' problem. Whenever a spurious event perturbs the trajectories of the proof masses, data analysis pipelines will have to be recalibrated; the geodesic equations will have to be re-solved for the positions and velocities of the individual proof masses, and accurate knowledge of their positions will grow as a function of elapsed mission time after re-solving the equations. In some instances it is possible to prevent or delay inopportune spurious accelerations (such as those associated with sciencecraft maintenance), which may be desirable to protect certain science objectives of the mission [6, 7]. In these cases, a well-modeled knowledge of the kinematics of the individual proof masses in response to a spurious acceleration can be used to expedite the re-solving procedure.

Previous considerations of spurious acceleration noise have been made in the context of simple estimates of the effect of minor bodies or dust passing near a LISA sciencecraft [8], searches for compact dark matter in the solar system [9] or general perturbations from a large passing mass or asteroid [10]. This paper develops a general, three-dimensional treatment to model burst accelerations on both proof masses in a single LISA sciencecraft for an arbitrarily oriented encounter with a perturbing mass. This formalism will be applied in future work to model disturbances in simulated LISA data streams produced by end-to-end simulators such as `Synthetic LISA` [11], `The LISA Simulator` [12] and `LISACode` [13]. These simulator environments are being used to generate publicly distributed mock LISA data streams for data analysis efforts. These simulated data streams are hosted online [14, 15] and form the basis for LISA data analysis challenges [16–20]. These data challenges are designed to test and extend analysis capabilities aimed at recognizing and characterizing astrophysical sources of gravitational waves. Future challenges will be designed to characterize and test algorithms in more realistic data streams containing instrument effects (data gaps, spurious noise, correlated noise, etc), such as those described in this paper.

The paper will be organized as follows. Section 2 will describe the acceleration profile of a single encounter between a particle and a LISA sciencecraft, which will form the foundation for later calculations. Section 3 will apply these general results in example applications, including the case of a shift of the sciencecraft's mass (e.g., when the thrusters fire to reposition the sciencecraft). Section 3.3 will describe populations of solar system particulates and will estimate the rate of acceleration events associated with those populations. The limitations of our model are discussed in section 4. Implications for spaceborne gravitational wave observatories and directions for future work are described in section 5.

2. Theory of single encounters

Spaceborne gravitational wave observatories will operate as constellations of 'drag-free' sciencecraft. The sciencecraft shelter and protect small free flying test masses (also called 'proof masses') which nominally play the role of the end mirrors in a laser interferometer. The sciencecraft isolate these test masses from external forces so that the masses move only on geodesics of the background spacetime. When a gravitational wave passes through the observatory, the ripples in the spacetime curvature change the proper distance between these test masses. This can be sensed using laser interferometry. Spurious perturbing forces, such

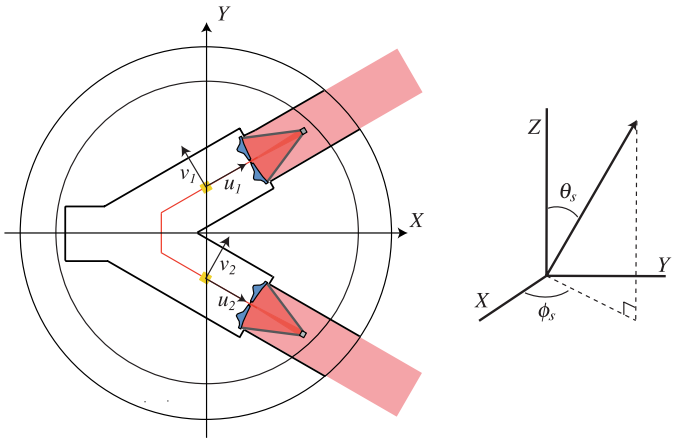

Figure 1. Several coordinate systems used in this paper. On the left is a schematic of the LISA sciencecraft. The origin of the *XYZ* frame (the 'sciencecraft frame') is the center of the sciencecraft, with the *X*-axis bisecting the angle between the beams. The *Z*-axis (not shown) comes out of the page and is considered to be the 'sunward' axis. The $(uvw)_i$ frames ('proof mass frames') are centered at the proof mass locations, with the u_i-axes along the beams and w_i parallel to *Z*. The LISA schematic is adapted from [8]. On the right, the sciencecraft's *XYZ* frame is shown again with spherical angles θ_s and ϕ_s shown.

(This figure is in colour only in the electronic version)

as near field fluctuations in the gravitational potential due to nearby masses, contaminate this measurement and are a source of noise that must be modeled.

2.1. Gravitational signature of perturbing masses

Consider the case of a single particle of mass m passing near a LISA sciencecraft. Assume that the relative velocity $\mathbf{v}$ and the point of closest approach $\mathbf{b}_m$ are known in the LISA sciencecraft frame (the *XYZ* coordinate system in figure 1). This frame is chosen such that the $+X$-axis bisects the angle between the beams and the $+Z$-axis points up through the sun-shield of the sciencecraft.

From these quantities there is enough information to calculate the trajectory of the particle in the LISA sciencecraft frame (assuming $t = 0$ when the particle is at the point of closest approach). Specifically, the vector position of a perturbing mass is

$$\mathbf{P}(t) = \mathbf{v}t + \mathbf{b}_m. \tag{1}$$

To calculate the acceleration of the proof masses (as a function of time) as the particle passes the sciencecraft, it is useful to transform to frames centered on the proof masses ($u_1v_1w_1$ or $u_2v_2w_2$ in figure 1). The $u_iv_iw_i$ frames are chosen to correspond to the faces of the cubic proof masses, with the u_i-axis along the beam and w_i parallel to *Z*.

The transformation from the sciencecraft frame to a proof mass frame consists of a rotation and a translation. Let β represent the angle between the *X*-axis and the equivalent axis in the proof mass frame (u_i), and let $\mathbf{r}_i$ be the position of the center of the proof mass in the *XYZ* frame[3]. Then the vector position of the perturbing mass in the proof mass frame is

$$\mathbf{p}_i(t) = R(\beta)[\mathbf{P}(t) - \mathbf{r}_i(t)], \tag{2}$$

[3] Based on the schematic in figure 1, the analyses in this paper will assume the proof masses lie on the *Y*-axis of the sciencecraft frame: $\mathbf{r}_i = \{0, \pm r_o, 0\}$.

where

$$R(\beta) = \begin{pmatrix} \cos\beta & \sin\beta & 0 \\ -\sin\beta & \cos\beta & 0 \\ 0 & 0 & 1 \end{pmatrix} \tag{3}$$

is a rotation matrix characterizing a rotation by angle β around the Z-axis of the sciencecraft. In a nominal LISA configuration, the rotation angles are $\beta_1 = +\pi/6$ and $\beta_2 = -\pi/6$.

If the perturbing mass' trajectory is written in the sciencecraft frame (XYZ) and each point is transformed in this manner, then the trajectory will be expressed from the viewpoint of a single proof mass, and the acceleration the proof mass experiences can be calculated as a function of time. For a given proof mass, the acceleration in the beam direction (along the u_i axis) is expressed as

$$a_u = \ddot{p}_u = \frac{Gm}{r^2}\frac{p_u}{r} = \frac{Gmp_u}{\left(p_u^2 + p_v^2 + p_w^2\right)^{3/2}}, \tag{4}$$

where r is the distance of the perturbing mass from the proof mass and G is the gravitational constant.

Note that the i subscripts have been suppressed for clarity in this expression; the expression is the same for either proof mass. Similar expressions can be found for $a_v = \ddot{p}_v$ and $a_w = \ddot{p}_w$. Expressing this as a general acceleration vector on the proof mass yields (again with subscripts i suppressed)

$$\ddot{\mathbf{p}}(t) = \frac{Gm\mathbf{p}(t)}{|\mathbf{p}(t)|^{3/2}} = \frac{Gm}{|\mathbf{p}(t)|^2}\widehat{\mathbf{p}}(t), \tag{5}$$

where $|\mathbf{p}(t)|^2 = \mathbf{p}(t)\cdot\mathbf{p}(t)$ is the magnitude of the position vector $\mathbf{p}(t)$ and $\widehat{\mathbf{p}}(t)$ is a unit vector that points toward the perturbing mass at any instant of time.

2.2. *Acceleration power spectra*

The acceleration of a LISA sciencecraft will have a time-dependent profile $a(t)$ along any given axis. The drag-free subsystems on the sciencecraft are designed to nullify the acceleration noise profile to a tolerable level. This will allow precise measurements to be made in the LISA's primary science band at frequencies $10^{-4} \lesssim f \lesssim 0.1$ Hz. Any residual acceleration not nullified by the drag-free system will, in principle, be detectable and will enter the science data stream as noise that competes with astrophysical gravitational wave signals. Acceleration noise is the dominant source of instrumental noise in LISA below $f \simeq 3\times10^{-3}$ Hz [8], making it the dominant factor in shaping the sensitivity of the observatory at these frequencies [1–4]. Acceleration noise is usually treated as a continuous random variable that contributes to the overall noise. Bursts of acceleration noise are generally localized in time and can masquerade as signal in the instrumental data record. Identifying events through a series of vetoes will be an essential part of any science analysis procedure.

In general, however, physical processes which cause bursts of acceleration on the proof masses will occur at some rate, where the number of expected events in any given time interval is governed by Poisson statistics. Over the entire LISA data record then, the ensemble of bursts can be treated as a well-defined stationary process which will contribute to the acceleration noise of the instrument. An acceleration event on an interferometer proof mass, $a(t)$, produces an apparent signal in the interferometer data stream of the form $\ddot{h}(t) = a(t)/L$, where L is the interferometer armlength. Writing this signal in the Fourier domain yields

$$\tilde{h}(f) = \frac{1}{(2\pi f)^2}\frac{\tilde{a}(f)}{L}, \tag{6}$$

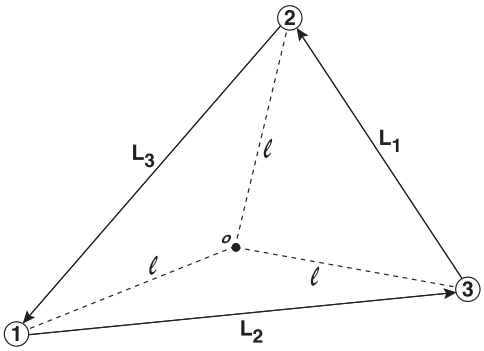

Figure 2. Schematic of the LISA constellation, illustrating the naming scheme used to write down the TDI variables (following [3]). In this notation, the numerical indices denoting sciencecraft or arms obey the standard permutation symmetry between TDI variables. The armlengths L_i are expressed in seconds; the guiding center distance, ℓ, defines a point o which is equidistant from each of the three sciencecraft.

where $\tilde{a}(f)$ is the Fourier transform of $a(t)$. The power spectral density of the signal $a(t)$, with Fourier transform $\tilde{a}(f)$, is defined as $S_a(f) = \Gamma \cdot \tilde{a}(f)\tilde{a}(f)^*$, where the asterisk denotes the complex conjugate. Γ is the expected rate of events, so $S_a(f)$ represents the ensemble average power of the bursts. Together with equation (6), the power spectral density of the dimensionless strain produced by acceleration events $a(t)$ is

$$S_h(f) = \frac{S_a(f)}{(2\pi f)^4 L^2}, \tag{7}$$

where f is the frequency of interest, L is the armlength of the interferometer and $S_a(f)$ is the power spectral density of the acceleration, which characterizes the amount of time variation in the acceleration $a(t)$ at a given frequency.

2.3. Effect on TDI variables

A perturbing acceleration event on one of the sciencecraft will manifest itself in the time series records of the time-delay interferometry (TDI) variables that are the fundamental interferometry signals for LISA [3]. Consider the Michelson-like signals, $\mathcal{X}(t)$ and $\mathcal{Y}(t)$, formed from the one-way laser links in two of the three arms and extracted from one of the vertexes of the constellation. Following the notation of [3] illustrated in figure 2, the TDI data streams can be described in terms of the Doppler shifts on individual laser links, $y_{ij}(t)$ received at spacecraft j down the arm i, and the individual armlengths in the constellation, L_i, expressed in seconds. Time delays in multiples of the armlengths are denoted using the 'comma notation': $y_{31,2} = y_{31}(t - L_2)$, $y_{31,23} = y_{31}(t - L_2 - L_3)$, etc. In this notation, the basic variables are written as follows:

$$\begin{aligned} \mathcal{X}(t) &= y_{32,322} - y_{23,233} + y_{31,22} - y_{21,33} + y_{23,2} - y_{32,3} + y_{21} - y_{31}, \\ \mathcal{Y}(t) &= y_{13,133} - y_{31,311} + y_{12,33} - y_{32,11} + y_{31,3} - y_{13,1} + y_{32} - y_{12}. \end{aligned} \tag{8}$$

Note that $\mathcal{X}(t)$ contains only laser links on arms 2 and 3, whereas $\mathcal{Y}(t)$ contains laser links on arms 1 and 3—the two variables share one arm in common.

Ignoring all sources of noise except the spurious accelerations of interest here, the contributions to the Doppler shift on a single laser link will contain a contribution from

the gravitational wave and the spurious acceleration, $y_{ij}(t) = y_{ij}^{\rm gw}(t) + y_{ij}^{\rm accel}(t)$. The acceleration term will depend on the spurious velocity induced by an acceleration. If $\vec{v}_{ij}(t)$ is the spurious velocity at spacecraft i on proof mass j (where $j = 1, 2$, as per the labeling in figure 1), there are two contributions to the acceleration on each link (one from each end of the arm). Consider a perturbation to sciencecraft 1 in figure 2, which is the vertex where $\mathcal{X}(t)$ is extracted. The two general acceleration terms from the links down arm 2 and arm 3 are

$$\begin{aligned} y_{21}^{\rm accel}(t) &= -\hat{n}_2 \cdot \vec{v}_{31}(t - L_2) + \hat{n}_2 \cdot \vec{v}_{12}(t), \\ y_{31}^{\rm accel}(t) &= \hat{n}_3 \cdot \vec{v}_{22}(t - L_3) - \hat{n}_3 \cdot \vec{v}_{11}(t), \end{aligned} \tag{9}$$

where $\hat{n}_i$ is the unit vector pointing down arm i with the directionality indicated by the arrows in figure 2. By contrast, $\mathcal{Y}(t)$ is extracted at the vertex formed by sciencecraft 2. The general acceleration terms from the links down arm 1 and 3 are

$$\begin{aligned} y_{32}^{\rm accel}(t) &= -\hat{n}_3 \cdot \vec{v}_{11}(t - L_3) + \hat{n}_3 \cdot \vec{v}_{22}(t), \\ y_{12}^{\rm accel}(t) &= \hat{n}_1 \cdot \vec{v}_{32}(t - L_1) - \hat{n}_1 \cdot \vec{v}_{21}(t). \end{aligned} \tag{10}$$

If an acceleration perturbation only affects sciencecraft 1, then only the v_{1i} terms in equations (9) and (10) survive, leaving

$$y_{21}^{\rm accel}(t) = \hat{n}_2 \cdot \vec{v}_{12}(t), \qquad y_{31}^{\rm accel}(t) = -\hat{n}_3 \cdot \vec{v}_{11}(t), \qquad y_{32}^{\rm accel}(t) = -\hat{n}_3 \cdot \vec{v}_{11}(t - L_3). \tag{11}$$

Note that a perturbation near the $\mathcal{X}(t)$ vertex sciencecraft will produce spurious accelerations in both arms used to generate the $\mathcal{X}(t)$ data but only one arm in the $\mathcal{Y}(t)$ signal (time-delayed by the light travel time down the arm). The velocities in equation (11) are simply time integrals of the general perturbing acceleration given in equation (5). Once the velocity resulting from a spurious acceleration event is known, the individual laser links are propagated through the full eight-pulse response to produce the resulting spurious signal in the $\mathcal{X}(t)$ and $\mathcal{Y}(t)$ signals. Vinet [10] wrote down the contribution of spurious acceleration events to the power spectral density of $\mathcal{X}(t)$ by approximating $v_{11}(t) = v_{12}(t)$, allowing the form of the FFT to be deduced for the geometry of his problem; he did not consider the one arm contribution to the $\mathcal{Y}(t)$ signal. Here, the full TDI form has not been evaluated explicitly from the laser links because the raw input into LISA simulation software will be the unprocessed acceleration profiles.

It should also be noted that the characteristics of the acceleration events (namely the velocity vector of the perturbing mass and the impact parameter) are encoded in the TDI variables in the form of the velocities $\vec{v}_{1i}(t)$, and it may be possible to exploit the appearance of the event in more than one TDI variable to reconstruct the parameters of the perturbing mass. Exactly similar considerations can be made for the last TDI variable, $\mathcal{Z}(t)$; expressions may be obtained by applying the standard permutation symmetry.

The velocities $\vec{v}_{ij}(t)$ are the velocity profiles for *individual proof masses*; a complete TDI treatment (carried out *ab initio* by LISA simulation software) will mix the perturbations on two or more proof masses. In the next section, a general treatment for deriving the velocity profile of either proof mass in response to a perturbation is developed. These individual corrections may be employed in a fully realized TDI simulation in accordance with equation (11).

3. Applications of this formalism

In this section, several simple examples are considered to illustrate the use of the formalism presented above, including encounters with solar system debris (such as meteor streams) and a shift of the sciencecraft center of mass (such as after a thruster has been fired). These kinds

of 'typical' events that a LISA sciencecraft may encounter represent the initial conditions which will be needed to apply recalibration procedures that solve for the dynamics of the proof masses as part of the LISA science analysis pipeline.

These examples are admittedly simplified and do not represent the complex control laws which will be required to control and evaluate the sciencecraft environment. They do, however, illustrate the problems and acceleration profiles which will have to be overcome as part of the science analysis procedure and provide a framework for explorations in this vein.

3.1. Perturbing mass flyby

Consider a simple example to illustrate the acceleration profile produced by the method described above. A particle of mass m moves on a path parallel to the Z-axis, with closest approach vector $\mathbf{b}_m = \{b_o, 0, 0\}$ and relative velocity $\mathbf{v} = \{0, 0, v_o\}$. From the viewpoint of proof mass $i = 1$, located at $\mathbf{r}_i = \{0, r_o, 0\}$ with rotation angle $\beta_i = +\pi/6$, the trajectory of this particle is found from equation (2) to be

$$p_{u1} = \frac{\sqrt{3}}{2} b_o - \frac{1}{2} r_o, \tag{12a}$$

$$p_{v1} = -\frac{1}{2} b_o - \frac{\sqrt{3}}{2} r_o, \tag{12b}$$

$$p_{w1} = v_o\, t. \tag{12c}$$

Then the acceleration experienced by proof mass 1 is given by equation (5) as

$$\ddot{p}_{u1} = \frac{Gm(\sqrt{3} b_o - r_o)}{2\left[b_o^2 + r_o^2 + v^2 t^2\right]^{3/2}}, \tag{13a}$$

$$\ddot{p}_{v1} = \frac{Gm(-b_o - \sqrt{3} r_o)}{2\left[b_o^2 + r_o^2 + v^2 t^2\right]^{3/2}}, \tag{13b}$$

$$\ddot{p}_{w1} = \frac{Gm v_o t}{\left[b_o^2 + r_o^2 + v^2 t^2\right]^{3/2}}. \tag{13c}$$

These acceleration profiles are shown in figure 3. This derivation reduces to the results derived by Vinet [10] for the special case of $b_o = D$, $\beta = 0$ and $r_o = 0$. Note that in Vinet's derivation, the acceleration is computed at the center of mass of a LISA sciencecraft, not at the location of individual proof masses.

For each component of the acceleration in figure 3, the corresponding Fourier transform amplitude profile can be computed to illustrate the contribution of the acceleration signals at different frequencies. Figure 4 plots $|\tilde{a}(f)|$, the square root of the Fourier power spectrum $\tilde{a}(f)\tilde{a}(f)^*$, for each component. The critical component of the acceleration in the LISA experiment will be the value along the optical axis of the individual LISA arms (u_1 for this example) because this is the direction along which the instrument senses the perturbing effects of passing gravitational waves.

Burst events, such as the one in this simple example, can masquerade in the LISA data as legitimate signals. Data analysis strategies to veto such signal events need to be developed and assessed to handle these types of events. Null data channels that suppress the gravitational wave signal in data streams, such as the symmetrized Sagnac channel ζ [22, 23] and the

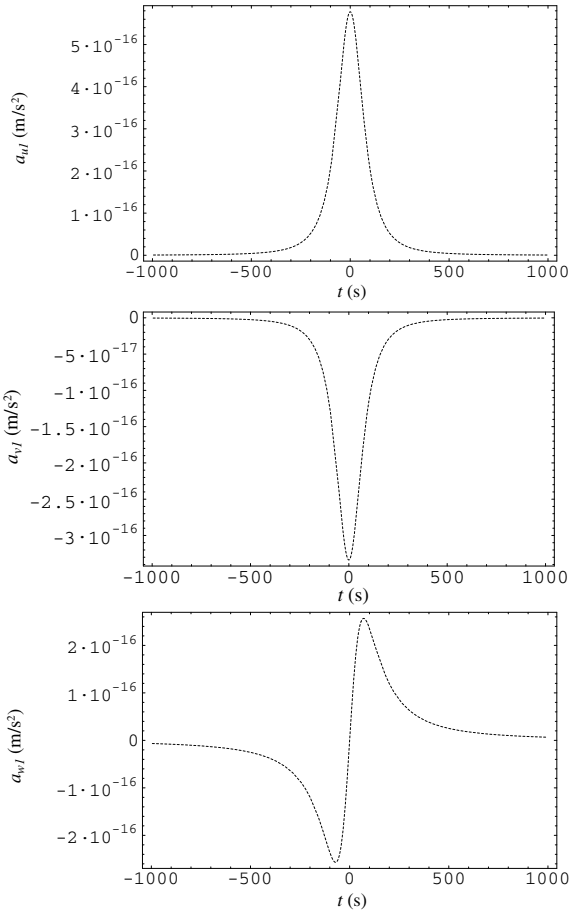

Figure 3. Acceleration profiles for the 'simple example' of a single particle passing by the LISA sciencecraft, as described in section 3.1. In this case, a 10 kg mass particle is traveling with speed $v_o = 10$ m s^{-1} parallel to the Z-axis (from negative to positive) and the point of closest approach is located on the positive X-axis at distance $b_o = 1000$ m. These profiles are shown in the uvw frame of proof mass 1. The profiles for the other proof mass are similar.

zero-signal solution [24, 25], are expected to be useful for vetoes of non-gravitational wave events for LISA. Those techniques, however, are only workable at low-frequencies, below the LISA transfer frequency, $f_* = c/(2\pi L) \sim 10$ mHz. However, given a wide range of plausible parameters of a perturbative mass, it is not unreasonable to expect that higher frequency events are plausible. For events that produce a significant amount of power at higher frequencies, the contributions to the noise are out of the nominal LISA band.

3.2. Sciencecraft center of mass shift

The drag-free system of the LISA sciencecraft is a feedback system which monitors the location of the proof masses (nominally moving only under the influence of gravity) and attempts to keep the sciencecraft centered on the proof masses by firing a system of micro-Newton thrusters distributed around the sciencecraft. Each time a thruster fires, the center of mass of the sciencecraft shifts by some small amount; as a consequence, there will be a small

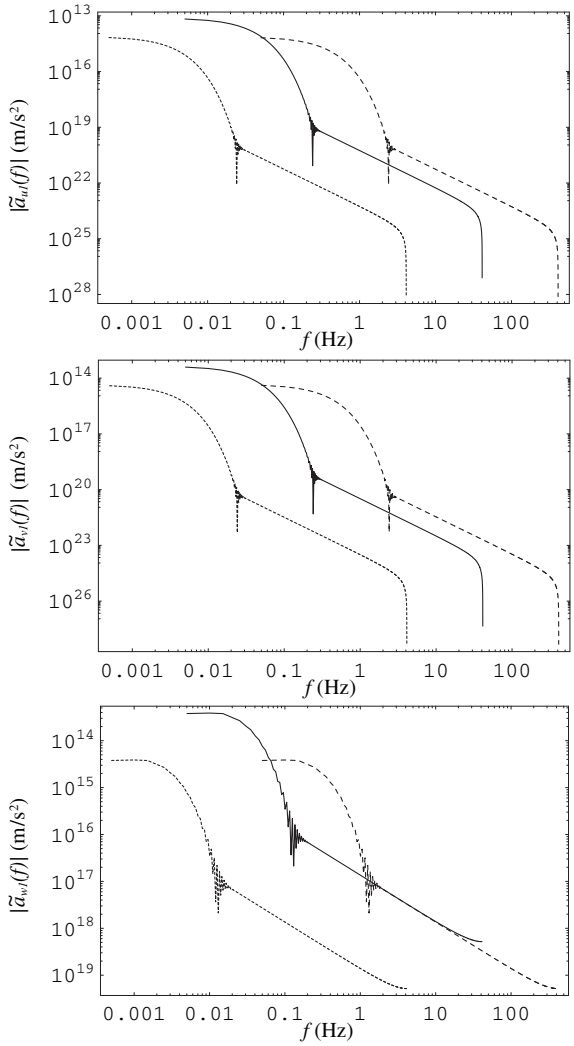

Figure 4. $\sqrt{|\tilde{a}(f)|^2}$ for sample acceleration profiles similar to those shown in figure 3. The three lines correspond to ($b_o = 10$ m, $m = 10^{-3}$ kg) for the solid line, ($b_o = 100$ m, $m = 1$ kg) for the dashed line and ($b_o = 1000$ m, $m = 10$ kg) for the dotted line (the case of figure 3). In all cases, $v_o = 10$ m s^{-1}.

acceleration imparted on each of the proof masses. The acceleration profile of a proof mass from the movement of the sciencecraft's center of mass can be computed using the formalism outlined above.

As an example of the center of mass shift, imagine a velocity profile that is parallel to the X-axis, as if the sciencecraft were attempting to stay centered on proof mass 1 in figure 1. The drag-free system of the sciencecraft capacitively senses a drift of the proof mass in the $+X$ direction and fires some combination of thrusters to move the craft in that direction. The sciencecraft moves in that direction until it is re-centered on the proof mass and then nulls the craft velocity by firing another thruster (or combination of thrusters). In reality the control

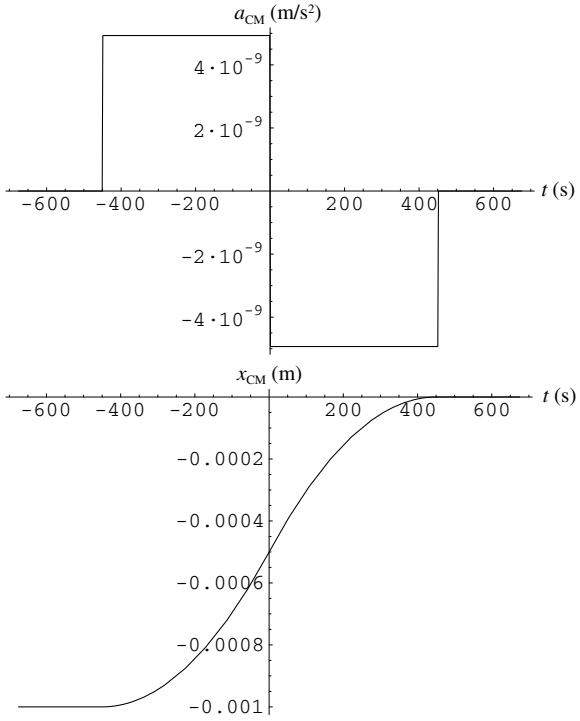

Figure 5. The simple acceleration and position profiles of a thruster maneuver to move the sciencecraft by 1 mm, as described in section 3.2.

laws governing the shift of the sciencecraft will reference *both* proof masses and attempt to stay centered on the pair simultaneously, but such an implementation is beyond the scope of this paper; here we consider only shifts following a single proof mass as an exercise to understand the types of acceleration profiles that the system will experience.

To see the gravitational effects of the shift of the sciencecraft's center of mass due to this type of thruster maneuver, assume that a thruster on one side of the sciencecraft fires for a period of time T, and then another thruster on the opposite side of the sciencecraft fires for the same period of time for braking. In both instances, assume that the thrusters turn on instantly and that the thruster fires at its maximum thrust $F_b = 1\ \mu$N. These assumptions should be valid since the rise time for the thrusters from zero to maximum thrust is ∼10–30 ms [26], which is usually going to be much smaller than the firing time T (as will be shown below). Then the acceleration of the sciencecraft's center of mass is

$$a_{\mathrm{CM}}(t) = \begin{cases} A, & -T < t < 0 \\ -A, & 0 < t < T \\ 0, & \text{else} \end{cases} \tag{14}$$

where $A = F_b/m_{\mathrm{LISA}}$ is the acceleration of the sciencecraft and $m_{\mathrm{LISA}} = 202.8$ kg is the mass of the sciencecraft.

For simplicity, we will consider only one proof mass, which has drifted a distance d in the $+X$ direction. Consequently, the thruster will fire to move the sciencecraft in the $+X$ direction. Integrating equation (14) twice with the assumption that the resulting functions

must be continuous and that the maneuver ends with the sciencecraft in the nominal position with respect to the proof mass (i.e., the proof mass is in the center of its cage) gives

$$x_{\mathrm{CM}}(t) = \begin{cases} -d, & t \leqslant -T \\ \frac{d}{2}\left[\left(\frac{t}{T}\right)^2 + 2\left(\frac{t}{T}\right) - 1\right], & -T < t \leqslant 0 \\ -\frac{d}{2}\left[\left(\frac{t}{T}\right)^2 - 2\left(\frac{t}{T}\right) + 1\right], & 0 < t \leqslant T \\ 0, & t > T. \end{cases} \tag{15}$$

The distance d of the center of mass shift is $\Delta x_{\mathrm{CM}} = d = AT^2$, which means that the thruster firing time for such a shift is

$$T = \sqrt{\frac{m_{\mathrm{LISA}} d}{F_b}}. \tag{16}$$

From this, it can be seen that the firing time is much longer than the rise time of the thrusters for center of mass shifts larger than nanometer scale.

To relate this to the previously described formalism, one can view equation (15) as a perturbation to the usual relationship between the proof mass and the center of mass. The location of the proof mass in the center of mass frame is specified by the vector $\mathbf{r}_1(t)$. If the nominal location of the proof mass is $\mathbf{r}_1(t) = \{0, r_o, 0\}$, then with the perturbation in this example, the location of the proof mass is

$$\mathbf{r}_1(t) = \{-x_{\mathrm{CM}}(t), r_o, 0\}. \tag{17}$$

Note that, for $t < -T$, this equation indicates that the proof mass is displaced from its nominal location by a distance d in the $+X$ direction, as was assumed for this example.

To apply the formalism, it is also necessary to know the location of the perturbing mass in the center of mass frame. Since the perturbing mass is effectively located at the center of mass,

$$\mathbf{P}(t) = \mathbf{b}_m = \{0, 0, 0\}. \tag{18}$$

Now equations (17) and (18) can be plugged into equations (2) and (5) to find the resulting acceleration experienced by the proof masses. The acceleration and Fourier amplitude profiles $|\tilde{a}(f)|$ for this example are shown in figures 6 and 7 for a 1 mm shift[4].

In the context of the example presented here, due consideration must be made regarding the effective mass distribution of the sciencecraft in the context of calculating its gravitational force on the proof mass. Since the final configuration of LISA is not yet known, a fully realized mass 'map' of the sciencecraft does not yet exist. For the purposes of this example, we have assumed that the mass of the sciencecraft is uniformly distributed and that only the mass located at a radius less than that of the proof mass effectively contributed to the force (cf Gauss's Law). This assumption results in a net gravity gradient at the proof mass even when it is in its nominal location (along the $+Y$-axis, noted in figure 1). This non-zero gravity gradient has been subtracted out of the results shown here, under the expectation that LISA will be designed to minimize local gravitational gradients when the proof masses are in their nominal location. Consequently, the results shown here should be considered as an estimate of the strength and frequency of this type of burst noise. Once a detailed mass distribution of the LISA sciencecraft is known, the formalism can be used to more accurately model the acceleration noise from thruster maneuvers.

[4] This is a much larger shift than might ever be reasonably expected to be allowable on LISA but is suitable for illustration.

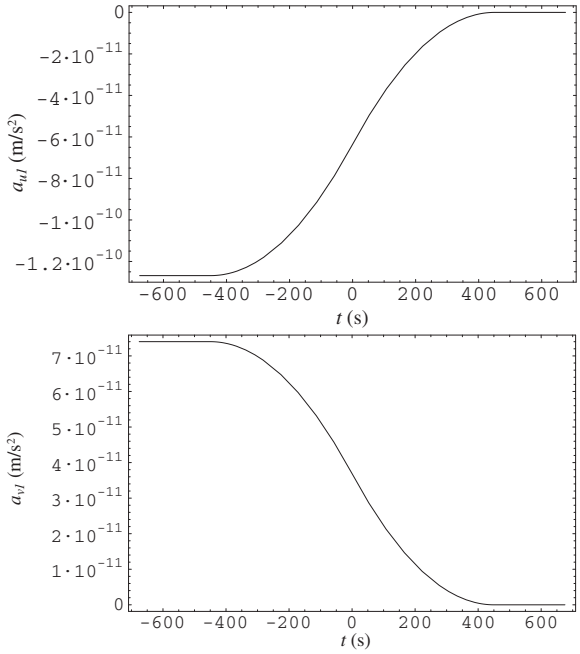

Figure 6. Sample acceleration profiles of a thruster maneuver in the $+X$ direction, as described in section 3.2, for an initial 1 mm offset. These profiles are shown in the uvw frame of proof mass 1; there is no acceleration in the w direction.

The shift in this example has been confined to the plane of the LISA sciencecraft. It is straightforward to generalize this for arbitrary thruster maneuvers. For a shift of magnitude d in an arbitrary direction given by the spherical coordinates (θ_s, ϕ_s) described in figure 1, the locations of the proof masses are

$$\mathbf{r}_1(t) = \{-x_{\mathrm{CM}}(t)\sin\theta_s\cos\phi_s,\, r_o - x_{\mathrm{CM}}(t)\sin\theta_s\sin\phi_s,\, -x_{\mathrm{CM}}(t)\cos\theta_s\}, \tag{19a}$$

$$\mathbf{r}_2(t) = \{-x_{\mathrm{CM}}(t)\sin\theta_s\cos\phi_s,\, -r_o - x_{\mathrm{CM}}(t)\sin\theta_s\sin\phi_s,\, -x_{\mathrm{CM}}(t)\cos\theta_s\}. \tag{19b}$$

Again, these and equation (18) can be plugged into equations (2) and (5) to find the resulting acceleration of the proof masses.

The nullification of a proof-mass offset (especially one as large as that shown in this example) must necessarily be an iterative process. The reason for this can be seen by considering figure 6. For some period of time, the proof mass will experience a non-zero acceleration due to the offset mass of the sciencecraft. Integrating this acceleration profile will give the velocity of the proof mass as a function of time. When the acceleration from the thruster goes to zero, the velocity of the proof mass is still non-zero, and of course, the proof mass will eventually drift off-station again, requiring a new corrective maneuver. Using the 1 mm offset of the above example, the proof mass would be left with a residual velocity of at least 6.6×10^{-8} m s^{-1}. (This number was calculated by integrating over the time of the maneuver only; the non-zero acceleration prior to the thruster maneuver will also contribute significantly to the velocity.) Over the course of 1 day, this translates into 5.7 mm drift. A 1×10^{-6} m offset yields a residual velocity of at least 2.1×10^{-12} m s^{-1},

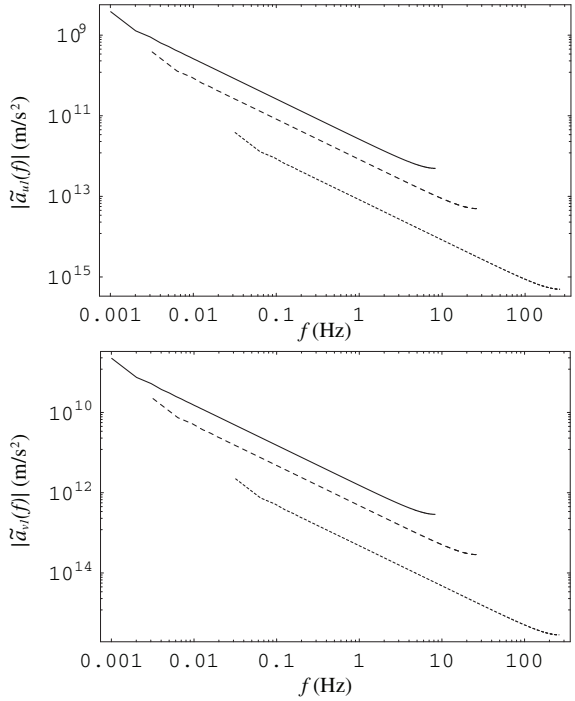

Figure 7. $\sqrt{|\tilde{a}(f)|^2}$ for the example acceleration profiles shown in figure 6. The three lines correspond to an initial $d = 1$ mm offset for the solid line, a $d = 0.1$ mm offset for the dashed line and a $d = 1\,\mu$ m offset for the dotted line.

which gives a 0.18 μm shift after one day. The optimal scheme for re-centering the proof masses in their nominal locations and nullifying the spurious velocity profiles that arise from the re-centering procedure has yet to be worked out and will be the subject of future work.

3.3. Debris in the solar system

The solar system is replete with small size material which is potentially detrimental to any space mission due to the potential risks of impacts. The problems are exacerbated for drag-free satellite systems such as LISA, where minute gravitational perturbations can contaminate the primary science signal. The particle content along the Earth's orbit is of principal concern, as LISA will be an Earth-trailing mission. It is plausible that a LISA sciencecraft will, on occasion, encounter small particles from the general background flux and from well-timed peaks with overdensities along the Earth's orbit (e.g., the known Earth-crossing meteor streams [30]).

As a model of the small particle background flux that will be encountered along the Earth's orbit, the yearly meteoroid influx onto the Earth has been derived from observations and tabulated in terms of number N as a function of mass [28]. For masses $m \lesssim 10^{-4}$ g, these data agree well with results from the Long Duration Exposure Facility [29]. To a good approximation, the particle fluxes are all geometric fluxes and are not dominated by the

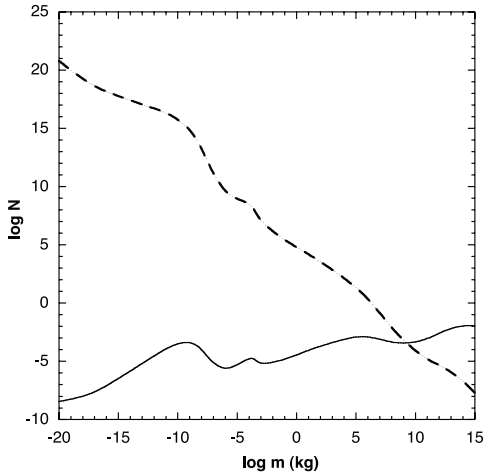

Figure 8. The number of 'significant' particles per year encountered by a *single* LISA sciencecraft along its orbit as a function of mass (solid line), computed via equation (22) and the Earth encounter data (dotted line). 'Significant' particles are deemed to be particles with enough mass passing close enough to the spacecraft to induce a proof mass acceleration greater than the threshold value of 3×10^{-15} m s^{-2}. Earth encounter data come from table XXVI of [28].

gravitational attraction of the Earth. As such, a good approximation of the LISA encounter rate N_L is obtained by simply scaling the geometrical cross section area of LISA to the Earth:

$$N_L = N\left(\frac{A_{\rm LISA}}{A_{\rm Earth}}\right) = N\left(\frac{R_{\rm LISA}}{R_{\rm Earth}}\right)^2, \tag{20}$$

where $R_{\rm LISA}$ is the encounter radius of interest around a LISA sciencecraft and $R_{\rm Earth}$ is the radius of the Earth. The radius of interest around a sciencecraft is defined by the threshold acceleration of interest, a_o. The critical distance $R_{\rm LISA}$ depends on the particle mass m and can be determined from a simple Newtonian estimate

$$a_o = \frac{Gm}{(R_{\rm LISA})^2}. \tag{21}$$

Solving this for $R_{\rm LISA}$ and substituting into equation (20) yields

$$N_L = \frac{NGm}{a_o R_{\rm Earth}^2}. \tag{22}$$

There is clearly a huge difference in the cross sectional area of the Earth compared to a LISA sciencecraft, so it is natural to ask whether a significant number of encounters will occur during a nominal LISA mission. The probability of k encounters with a single LISA sciencecraft in a year will be described by a Poisson distribution

$$P(k|N_L) = \frac{{\rm e}^{N_L} N_L^k}{k!}, \tag{23}$$

where the encounter rate per year (as a function of mass) is given by N_L, plotted in figure 8. The probability of an event crossing the threshold a_o during a year of LISA observations will simply be the sum of the probabilities $P(1|N_L)$ for each value of the mass[5]. The result of this

[5] The mass data used in figure 8 are given in discrete mass bins; this properly should be integrated over mass, if a functional form were known.

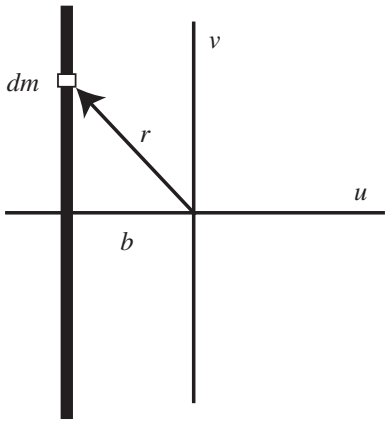

Figure 9. Schematic showing the orientation used for the 'linear mass' estimation. The coordinate system is the uvw system for a proof mass (hence, the proof mass under consideration is located at the origin). The meteor stream is approximated as a linear mass, shown as the thick black line here. The meteor stream is parallel to the v-axis and is moving in the $+w$ direction (out of the page). The stream is shown at time $t = 0$, when it is at its closest approach (minimum distance b) to the proof mass. To find the acceleration of the proof mass as a result of the passage of the line mass, the expression for the acceleration is integrated over the mass elements dm of the line mass.

calculation for a threshold of $a_o = 3 \times 10^{-15}$ m s^{-2} is 16.7%; for all three sciencecraft then, there is a 50% probability per year of an event occurring from random encounters with solar system debris.

Note that a rate of strikes from particles *hitting* the LISA sciencecraft could be estimated from equation (20) by simply setting R_{LISA} equal to the radius of the sciencecraft itself. It is expected that the burst of acceleration from a strike on the sciencecraft will produce high frequency noise from the sudden deceleration of the particle; this has been examined in the context of ground-based detectors [27] but not for LISA (though the noise may likely be out of band).

The particle flux from [28] includes the flux from individual Earth-crossing meteor streams. The properties of these streams have been determined through observations of meteor showers from the surface of the Earth. They are known to occur at well-known times and positions along the Earth's orbit, and their properties have been well documented in terms of the particle number density, mass, size and trajectory [30]. Since the flux from the known meteor streams is naturally a part of the total integrated flux, it is unlikely a detailed study of the streams will produce an increased number of particle encounters with a LISA sciencecraft (though the likelihood that the few expected encounters will happen during a crossing of a known stream is increased). However, it should be noted that the individual streams represent overdensities in the local mass distribution of small particles, and it is prudent to ask whether or not the cumulative effect of all the mass in a nearby stream can have a perturbing effect on a passing LISA sciencecraft.

To estimate the maximum magnitude of the collective effects, we can approximate the stream as a line mass (with linear density λ = mass/length) of length ℓ. Since this approximation is intended only to find the magnitude of the acceleration such a stream would cause, we will consider only one proof mass and assume for simplicity that the line mass is parallel to the v-axis and is traveling in the $+w$ direction with speed v_o. (See figure 9.) The

smallest distance b between the proof mass and the line mass occurs at time $t = 0$ and in the $-u$ direction.

Before continuing with this calculation, it should be noted that this method of calculating the collective gravitational effect of the stream is most accurate when the distance of closest approach is large compared to both the separation between the individual masses in the stream and the radius of the stream. The closest approach *is* significantly larger than the average particle separation in all of the sciencecraft encounters with the 57 streams for which we had appropriate data (from [30]). However, in most of these encounters, the closest approach distance was *less* than the swarm radius (meaning that the sciencecraft was passing through the stream). As a result, we can view this model as providing an *upper limit* on the collective gravitational effect of the stream because the gravitational force of particles on opposite sides of the sciencecraft will partially cancel, reducing the magnitude of the effect. In general, acceleration profiles of these encounters will appear to have some single-particle acceleration profiles superimposed on a 'background' collective-effect profile (which would have a shape similar to that produced when a sciencecraft passes through an extended cylinder of uniform mass density).

Since we are, at the moment, concerned with the question of whether the collective effect is significant, we can start by looking at the upper limits of the acceleration it can produce. Thus, we continue with the 'line-mass' calculation. To find the acceleration of the proof mass due to the passing line mass, we need to apply equation (5) to each mass element dm. The resulting component of the acceleration is

$$\mathbf{d\ddot{p}} = \frac{G\mathrm{d}m}{r^2}\hat{\mathbf{r}}, \tag{24}$$

where $\hat{\mathbf{r}}$ is the unit vector pointing from the origin to the location of the mass element dm and $r^2 = u^2 + v^2 + w^2$, where $u = -b$ and $w = v_o t$ in this case. The mass element can be expressed in terms of the linear mass density as

$$\mathrm{d}m = \lambda \mathrm{d}v. \tag{25}$$

Using this and geometry, the components of the acceleration are then integrated over the length ℓ of the line mass to give

$$\ddot{p}_u(t) = \frac{G\lambda b\ell}{\left(b^2 + v_o^2 t^2\right)\sqrt{b^2 + \frac{\ell^2}{4} + v_o^2 t^2}}, \tag{26a}$$

$$\ddot{p}_v(t) = 0, \tag{26b}$$

$$\ddot{p}_w(t) = \frac{G\lambda v_o t\ell}{\left(b^2 + v_o^2 t^2\right)\sqrt{b^2 + \frac{\ell^2}{4} + v_o^2 t^2}}. \tag{26c}$$

As expected from symmetry, the v-components cancel. The maximum of a_u will occur at $t = 0$, so that

$$a_{u,\max} = \frac{G\lambda\ell}{b\sqrt{\frac{\ell^2}{4} + b^2}}. \tag{27}$$

Note that this expression is asymptotic as the length ℓ increases. One could choose an appropriate ℓ based on how close a_u gets to the asymptotic value.

Finding the maximum amplitude of the acceleration from equations (26*a*)–(26*c*) gives an upper limit on the acceleration that the meteor stream can produce. In performing this analysis

on the encounters of each of the three LISA sciencecraft with the known meteor streams [30] for which we had appropriate data (57 streams), none of the streams produced a collective effect that was above the expected LISA threshold sensitivity. Over the course of one orbit, the encounters producing the largest collective effects were at least three orders of magnitude below threshold.

Here we have only considered particle flux close to an individual LISA sciencecraft. Using the same formalism, it is simple to show that the particle flux through an individual LISA laser link can be significantly larger if the link is modeled as a cylinder 30 cm in diameter and 5×10^6 km long. An important contribution to the LISA noise in this case will be phase noise from scattered laser light off transient particles; this will be the subject of future work.

4. Limits of the method

The method outlined in this paper has limitations in its application. First, it assumes an overly simple model for the mass distribution of a LISA sciencecraft and neglects to consider any of the rigid-body dynamics of the sciencecraft itself in response to external perturbations. These effects will certainly be of importance, but no well-established mass or material model of the LISA sciencecraft currently exists, making such considerations speculative at best. Furthermore, current LISA end-to-end simulators [11–13] are designed to simply track the LISA proof-masses. Noise is injected into the simulated data streams directly without modeling its physical origin and is propagated through the interferometry. The work presented here, while it neglects the sciencecraft rigid-body dynamics, should produce a reasonable estimate of the strength and spectrum of spurious bursts of acceleration noise that can be injected into these simulators.

Secondly, this paper assumes that a LISA sciencecraft can be treated as a small inertial laboratory, and non-inertial effects due to its orbital motion around the Sun can be neglected. The level at which non-inertial effects become important can be estimated by considering the equations of motion for a simple system comprised of LISA, a perturbing particle and the Sun. If the sciencecraft and perturbing mass are separated by a distance r and their center of mass is separated from the Sun by a distance R, the Lagrangian for the system may be expressed in terms of these two coordinates. The equations of motion describing the evolution of r (the LISA-particle interaction distance) and the evolution of R are uncoupled to $\mathcal{O}(r/R)^2$. In the limit then that $r \ll R$, the interaction of the perturbing particle with LISA can be treated as occurring in an inertial frame; for $r \sim 100$ m and $R = 1$ AU, the second-order terms are smaller than the lower-order terms by $\mathcal{O}(r/R)^2 \sim 10^{-19}$. The largest higher-order corrections at $\mathcal{O}(r/R)^2$ are tidal terms, but these perturbations occur with periods of a year (the LISA orbital timescale), much longer than the short duration of acceleration bursts caused by a passing perturbative mass.

5. Discussion

Future work related to this modeling will entail incorporating these results into full end-to-end LISA software models [11–13] as part of a modeling exercise to characterize how individual acceleration bursts on a sciencecraft's system of proof masses will propagate through the observatory interferometry and manifest itself in the output data streams. For a study of this sort, the models of the acceleration presented in equations (4)–(5) will be placed in a raw input stream for the simulators, and the resulting time stream analyzed to understand the impact of an acceleration burst on data analysis algorithms. This exercise will form the foundation of

a veto method which can be used as part of a standard science analysis pipeline. Work on modeling of data gaps is a major forthcoming effort in LISA data challenges, and it is expected that this formalism can be included as part of developing challenge sets available through the *Mock LISA Data Challenges* [15] and the *Testbed for LISA Analysis* [14].

Once a full model of the LISA sciencecraft has been decided, there are many applications which can utilize the framework presented here, particularly in the context of local gravity gradients on the sciencecraft. One obvious example is the motion of the LISA communications antennae. Several possible locations have been suggested for positioning the antenna on a sciencecraft [26], but in all cases the antenna will have to be moved occasionally to maintain contact with Earth. The mass of such a component will create a significant change in the local gravitational gradient on the proof masses and produce a large acceleration each time the antenna is moved. Modeling and understanding these acceleration profiles will be an essential part of processing the LISA science data, as each reconfiguration of the sciencecraft will require a recalibration of the proof-mass acceleration and velocity profiles, which are used in the construction of the primary interferometry variables. These resolution periods are part of the 'data-gap' and 'protected observing' problems in LISA science analysis [6, 7].

As was noted in section 3.1, the results presented here for the acceleration produced by a single perturbing mass reduce to those of Vinet [10], who considered the perturbing effects of asteroids. Vinet's calculation extends to include a derivation of the spectral noise density in individual LISA time-delay interferometry channels. While this could easily be included for the treatment presented here, it has not been done explicitly because the raw input into LISA simulation software will be the unprocessed acceleration profiles; interferometric noise densities of those profiles will be a natural output of the simulation software.

Acknowledgments

The authors would like to thank Ron Hellings and Kip Thorne for helpful comments and suggestions, and P Jenniskens for extensive meteor stream data beyond that found in [30]. They gratefully acknowledge support from the Center for Gravitational Wave Physics at Penn State, funded by the NSF under cooperative agreement PHY 01-14375. SLL also acknowledges support from NASA award NNG05GF71G.

References

[1] Larson S L, Hiscock W A and Hellings R W 2000 *Phys. Rev.* D **62** 062001
[2] Larson S L, Hellings R W and Hiscock W A 2002 *Phys. Rev.* D **66** 062001
[3] Armstrong J W, Estabrook F B and Tinto M 1999 *Astrophys. J.* **527** 814
[4] Estabrook F B, Tinto M and Armstrong J W 2000 *Phys. Rev.* D **62** 042002
[5] Phinney E S *et al* (LISA Working Group 1) 2002 LISA Science Requirements, white paper, available at http://www.srl.caltech.edu/lisa/
[6] Cornish N J 2005 Protected observing periods for LISA, white paper, available at http://www.srl.caltech.edu/lisa/
[7] Bender P *et al* (LISA Data Issues Task Force) 2005 LISA Data Issues, white paper, available at http://www.srl.caltech.edu/lisa/
[8] Bender P *et al* 1998 *LISA Pre-Phase A Report* 2nd edn (Garching: Max-Planck-Institut für Quantenoptik)
[9] Seto N and Cooray A 2004 *Phys. Rev.* D **70** 063512
[10] Vinet J-Y 2006 *Class. Quantum Grav.* **23** 4939
[11] Vallisneri M *Synthetic LISA* located at http://www.vallis.org/syntheticlisa/
based on Vallisneri M 2005 *Phys. Rev.* D **71** 022001
[12] The LISA Simulator located at http://physics.montana.edu/LISA/, based on Rubbo L J, Cornish N J and Poujade O 2004 *Phys. Rev.* D **69** 082003

[13] Petiteau A *et al* 2006 *Proc. 6th Int. LISA Symp., AIP Conf. Proc.* **873** 633
[14] *The Testbed for LISA Analysis (TLA)* http://tla.gravity.psu.edu/
[15] *The Mock LISA Data Challenges (MLDC)* http://astrogravs.nasa.gov/docs/mldc/
[16] Benacquista M J, Finn L S, Larson S L and Rubbo L J 2006 Addressing LISA Science Analysis Challenges, white paper *Preprint* gr-qc/0606089
[17] Finn L S, Benacquista M J, Larson S L and Rubbo L J 2006 *Proc. 6th Int. LISA Symp. AIP Conf. Proc.* **873** 640 (*Preprint* gr-qc/0602019)
[18] Arnaud K A *et al* (The Mock LISA Data Challenge Task Force) 2006 *Proc. 6th Int. LISA Symp., AIP Conf. Proc.* **873** 619
[19] Arnaud K A *et al* (The Mock LISA Data Challenge Task Force) 2007 *Class. Quantum Grav.* **24** S529 (*Preprint* gr-qc/0701139)
[20] Arnaud K A *et al* (The Mock LISA Data Challenge Task Force) 2007 *Class. Quantum Grav.* **24** S551 (*Preprint* gr-qc/0701170)
[21] Larson S L Online sensitivity curve generator http://www.srl.caltech.edu/~shane/sensitivity/, based on Larson S L, Hiscock W A and Hellings R W 2000 *Phys. Rev.* D **62** 062001
[22] Tinto M, Armstrong J W and Estabrook F B 2000 *Phys. Rev.* D **63** 021101
[23] Hogan C and Bender P 2001 *Phys. Rev.* D **64** 062002
[24] Tinto M and Larson S L 2004 *Phys. Rev.* D **70** 062002
[25] Tinto M and Larson S L 2005 *Class. Quantum Grav.* **22** S531
[26] Edwards T *et al* 2000 *LISA: Study of the Laser Interferometer Space Antenna: Final Technical Report* (FTR) (Dornier Satellitensysteme GmbH, DSS) (Report No LI-RP-DS-009)
[27] Creighton T 2000 *Preprint* gr-qc/0007050
[28] Ceplecha Z *et al* 1998 *Space Sci. Rev.* **84** 327
[29] Love S G and Brownlee D E 1993 *Science* **262** 550
[30] Jenniskens P 1994 *Astron. Astrophys.* **287** 990
Jenniskens P Private communication